

# Modelling and characterization of a pneumatically actuated peristaltic micropump

T. N. Gerasimenko

*M.V. Lomonosov Moscow State University, Faculty of Physics, Moscow, Russia*

O. V. Kindeeva, V. A. Petrov, A. I. Khaustov

*Moscow Aviation Institute, Moscow, Russia*

E. V. Trushkin

*Hemule GmbH, Berlin, Germany*

---

## Abstract

There is an emerging class of microfluidic bioreactors which possess long-term, closed circuit perfusion under sterile conditions with *in vivo*-like flow parameters. Integrated into microfluidics, peristaltic-like pneumatically actuated displacement micropumps are able to meet these requirements. We present a theoretical and experimental characterization of such pumps. In order to examine volume flow rate, we have developed a mathematical model describing membrane motion under external pressure. The viscoelasticity of the membrane and hydrodynamic resistance of the microfluidic channel have been taken into account. Unlike most similar models, the developed model implies only the physical parameters of the pump and allows the estimation of their impact on the resulting flow. The model has been validated experimentally.

*Keywords:* mathematical model, micropump, volume flow rate

*2010 MSC:* 74D05, 74F10,

---

## 1. Introduction

Various microfluidic systems were designed to recreate an *in vivo* microenvironment for cell cultures with regard to physiological mechanical stimulation [1], [2].

5 A pump providing the circulation of liquid is the key component of these devices [3]. A pump can be either external or integrated into a microfluidic chip [4], [5], [6]. A pump with a pulsatile flow creates significant variations in volume flow rate, affecting the cells by time-varying pressure and shear stress

---

*Email address:* gerasimenko@physics.msu.ru (T. N. Gerasimenko)

on the cells' surface [7], [8], [9], [6], [10]. Since the production of a pump is a  
10 complex process, it is required already at the design stage to understand how the  
parameters of a pump will affect the resulting flow. In general, fluid-structure  
interaction modelling is addressable only by numerical simulation [11], [12]. The  
lumped element model is traditionally used to simplify modelling when the pump  
is analyzed separately from the microfluidic system and its characteristics are  
15 taken as boundary conditions for a liquid flow simulation within a microchannel  
[13], [14].

A representation of a pump as an equivalent electric circuit is the most  
common approach for pump modelling [15], [16], [17], [18]. These methods  
result in flow parameters close to the experimental ones, however, the transition  
20 from the pump's physical parameters to the equivalent capacitance, resistance  
and inductivity is not clear enough. Thus the effect of pump characteristics on  
flow properties can only be roughly estimated. Moreover, specialized software  
is required when the equivalent scheme is too complex and branched [15], [19],  
[16].

25 The studied pump was a peristaltic-like displacement micropump consisting  
of two active valves with a working chamber in between. The valves and the  
working chamber were elastic, pneumatic-actuated membranes organized in a  
row along a microfluidic channel. Each valve membrane had a strap blocking  
the channel when the applied pressure was greater than atmospheric pressure  
30 (Fig. 1). The valves and the chamber were operated by the proprietary Hemule  
control unit making the pressure over the membranes either higher (closed valve)  
or lower (opened valve) than atmospheric pressure. The 6-step algorithm pre-  
sented in Fig. 2 was implemented in the control unit. All pressure values relate  
to atmospheric pressure. Frequency is a reciprocal value of one step duration.  
35 The six steps together correspond to a single working cycle.

Models of a similar pump have been presented by [20] and [21]. However,  
the proposed models include experimentally determined empirical parameters  
with unclear physical meaning thus the major factors affecting volume flow  
rate remained unidentified. Here we present a mathematical model elucidating  
40 how the membranes, microfluidic channel and control unit properties affect the  
characteristics of the pump.

## 2. Materials and methods

The micropumps were fabricated in 2 mm polydimethylsiloxane (PDMS)  
layer using soft lithography [22] and then bonded to a standard 1-mm microscopic  
45 glass slide by means of plasma treatment [23]. The other side of the PDMS layer  
was based on 10 mm polycarbonate plate with ports for fluidic and pneumatic  
connections as well as for pressure sensors (Fig. 1). Three versions of the pump  
were produced to analyze the impact of the pump geometry on its volume flow  
rate. Two of them (pump I and pump III) had valve diameters of 2.5 mm.  
50 Pump II had smaller valves with diameters of 2 mm. All three pumps had a  
chamber diameter of 2.5 mm (Fig. 3). The thickness  $h$  of the membranes was  
 $530 \pm 5 \mu\text{m}$  except for the chamber membrane of pump III ( $440 \pm 5 \mu\text{m}$ ). The

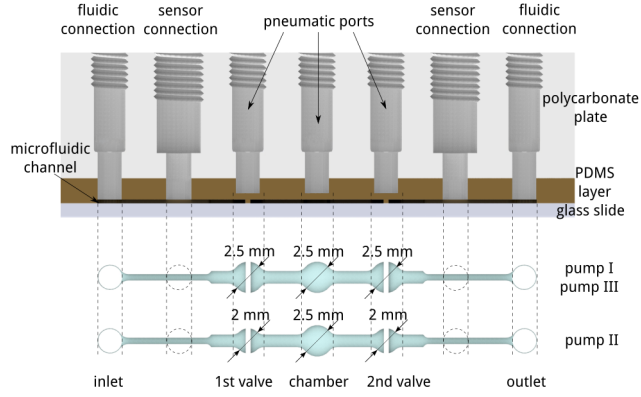


Figure 1: The studied micropumps. All three pumps have a chamber diameter of 2.5 mm and a valve membrane thickness of  $530 \pm 5 \mu\text{m}$ . Pump I and pump III have valve diameters of 2.5 mm. Pump II has valves with diameters of 2 mm. Pump I and pump II have chamber membrane thicknesses of  $530 \pm 5 \mu\text{m}$ . Pump III has a chamber membrane with a thickness of  $440 \pm 5 \mu\text{m}$ .

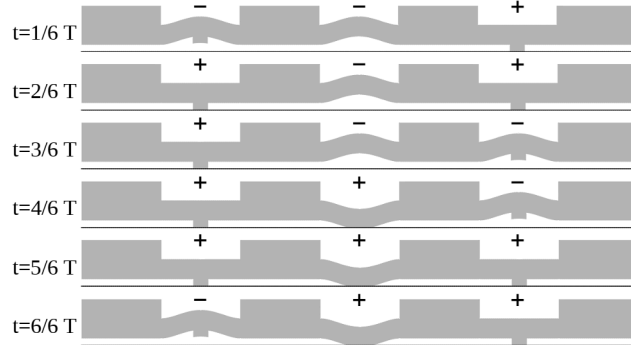


Figure 2: The 6-step algorithm

pneumatic chamber diameters over the membranes were 2 mm and the channel height was  $100 \mu\text{m}$  for all pumps.

PDMS viscoelastic properties were described according to the Kelvin-Voigt model, assuming the following stress-strain relation

$$\sigma(t) = E\varepsilon(t) + \eta\dot{\varepsilon}(t) \quad (1)$$

where  $\sigma(t)$  is stress,  $\varepsilon(t)$  is strain,  $E$  is the PDMS Young modulus and  $\eta$  is its viscosity. The Young modulus of the PDMS strongly depends on the method and conditions of the PDMS preparation [24], therefore we have estimated it by

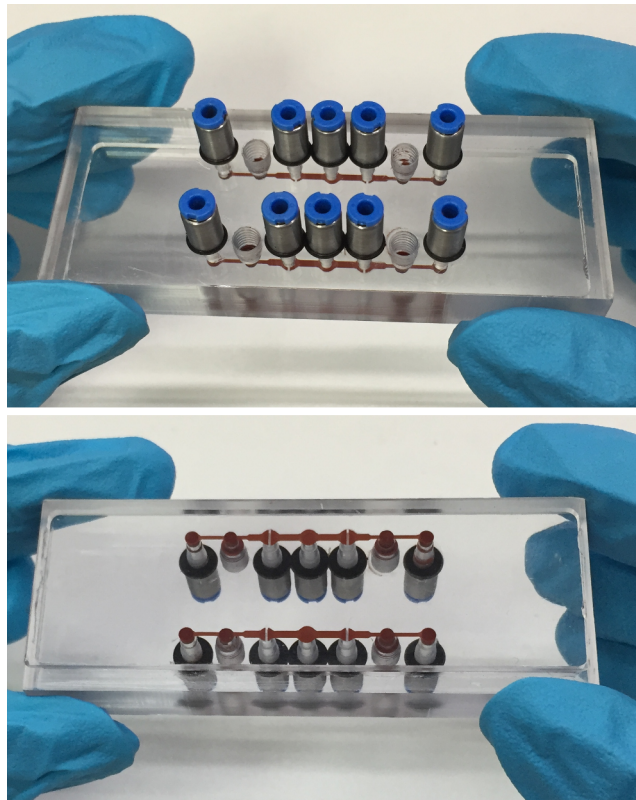


Figure 3: Photo of the device with pumps I and II

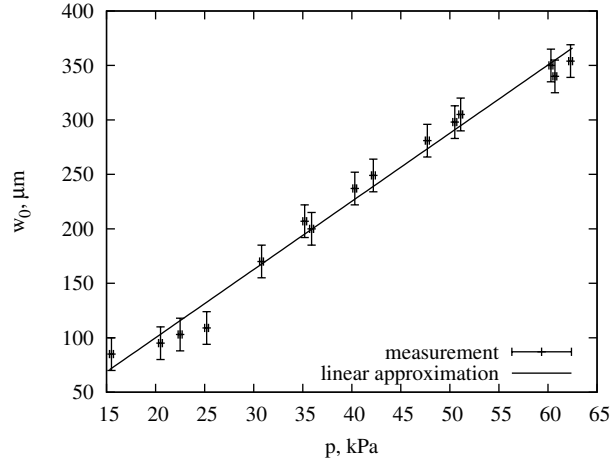


Figure 4: The experimental dependency of the membrane center deflection on the pressure value

a chamber membrane deflection under a static load as follows [25]:

$$E = \frac{3}{16} \frac{R^4}{h^3} (1 - \nu^2) \frac{p}{w_0}$$

55 where  $\nu = 0.499$  is the Poisson's ratio [24],  $w_0$  is the deflection of the membrane centre from its quiescent position, and  $p$  is the pressure over the membrane. In order to measure  $w_0$ , the pump was placed sideways on a stage of the inverted microscope. The static pressure over the working chamber membrane was adjusted using the control unit. The obtained relationship between the membrane  
 60 centre deflection and the pressure value was approximated by a linear function (Fig. 4).

The obtained Young modulus of  $760 \pm 140$  kPa was in good agreement with the results of [14] and [26].

### 3. Mathematical model

65 The developed mathematical model is based on the idea that the volume flow rate caused by each membrane motion can be determined by an integration of membrane velocity over its surface due to the no-slip conditions on a membrane boundary. The velocity has been obtained by solving a membrane motion equation. Since each membrane was actuated by air pressure in pneumatic tubes,  
 70 first we described the time-dependency of the air pressure.

#### 3.1. Time-dependence of the applied pressure

The positive and negative pressures inside the control unit were kept constant, therefore the transient processes of changing pressure were considered as

an efflux of air from/to an infinite reservoir according to [27]:

$$\frac{d\eta_{up}}{dt} = A\eta_{up}^{2/7}\sqrt{\eta_{up}^{-2/7} - 1} \quad (2)$$

$$\frac{d\eta_{dn}}{dt} = -A\eta_{dn}^{5/7}\sqrt{1 - \eta_{dn}^{2/7}} \quad (3)$$

for increase and decrease of the pressure correspondingly.  $\eta_{up/dn} = p_{up/dn}/p_0$ , where  $p_0$  is the pressure provided on the control unit outlets,  $p_{up/dn}$  describe the increasing and decreasing pressures correspondingly.

$$A = \frac{R_z\sqrt{T_k}b\tilde{S}\tilde{\mu}}{V}$$

$R_z = 287$  J/kg/K is the specific gas constant for dry air,  $T_k$  is air temperature,  $b = 0.155$  (kg K/J)<sup>1/2</sup> and  $\tilde{\mu} = 0.8$  are empirical coefficients [27],  $\tilde{S}$  is the cross-section of the control unit throttle orifice,  $V$  is the total volume of the pneumatic tube and the connection.

The solution of these equations gives the increasing pressure dependency on time in an implicit form:

$$(1 - \eta_{up}^{2/7})^{1/2} - \frac{2}{3}(1 - \eta_{up}^{2/7})^{3/2} + \frac{1}{5}(1 - \eta_{up}^{2/7})^{5/2} - (1 - \eta_0^{2/7})^{1/2} + \frac{2}{3}(1 - \eta_0^{2/7})^{3/2} - \frac{1}{5}(1 - \eta_0^{2/7})^{5/2} = -\frac{A}{7}(t - t_0) \quad (4)$$

and the decreasing one in an explicit form:

$$\eta_{dn} = \left[ 1 - \left( \sqrt{1 - \eta_0^{2/7}} + \frac{A}{7}(t - t_0) \right)^2 \right]^{7/2} \quad (5)$$

with  $\eta_0$  being a normalized pressure value at  $t_0$  for each case.

The pneumatic signal edges  $\Delta t_{up}$  and  $\Delta t_{dn}$  were obtained setting  $\eta_{up}(t_0 + \Delta t_{up}) = 1$  and  $\eta_{dn}(t_0 + \Delta t_{dn}) = 0$  as follows

$$\Delta t_{up} = \frac{7}{A} \left[ (1 - \eta_0^{2/7})^{1/2} - \frac{2}{3}(1 - \eta_0^{2/7})^{3/2} + \frac{1}{5}(1 - \eta_0^{2/7})^{5/2} \right] \quad (6)$$

$$\Delta t_{dn} = \frac{7}{A} \left( 1 - \sqrt{1 - \eta_0^{2/7}} \right)$$

Finally the pressure over a membrane was described by the piecewise function of the form:

$$p(t) = \begin{cases} 2p_0(\eta_{up}(t) - 0.5), & t_0 \leq t \leq t_0 + \Delta t_{up} \\ p_0, & t_0 + \Delta t_{up} < t < t_0 + \Delta t_{up} + \delta t \\ 2p_0(\eta_{dn}(t) - 0.5), & t_0 + \Delta t_{up} + \delta t \leq t \leq t_0 + \Delta t_{up} + \delta t + \Delta t_{dn} \\ \dots & \dots \end{cases} \quad (7)$$

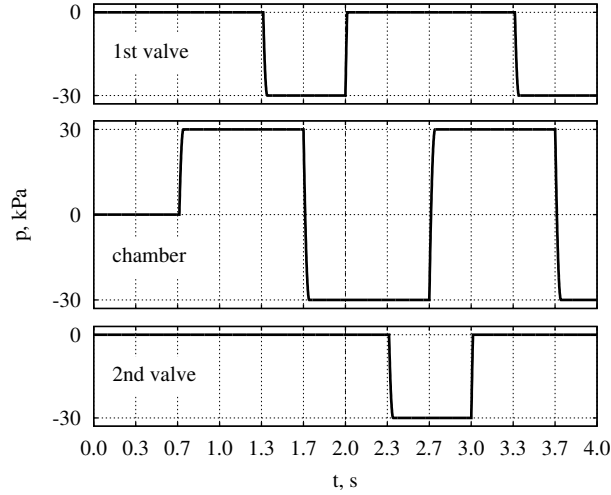


Figure 5: The dependency of the pressure over the valves and chamber membranes on time for  $p_0 = 30$  kPa and  $\nu = 3$  Hz control unit mode. The dashed line represents the beginning of the 6-step algorithm.

where  $\delta t$  is the time span when the pressure remains constant. We neglected possible deformations of valve halves after its strap comes into contact with the channel bottom and assumed that the valve fully stops. Therefore we substituted positive values of pressure bending the valve membrane with zero, since only the membrane bending and not its compression makes a contribution to the flow rate. Fig. 5 represents the corresponding pressures over the valve and chamber membrane for  $\pm 30$  kPa and 3 Hz control unit mode. The initial pressure values were assumed to be zero (all membranes are in the quiescent position) for the convenience of following calculations, therefore the 6-step working algorithm begins from 2 s.

### 3.2. Membrane motion

The membrane was assumed to be isotropic and shear deformations were neglected. Since the channel height was  $100 \mu\text{m}$  and the membrane thickness was about  $500 \mu\text{m}$ , its deflection from the quiescent position was assumed to be low. An application of a general theory for such circular membrane bending [25], [28] to the Kelvin-Voigt stress-strain relationship (1) gives the following initial and boundary value problem for a deflection of the membrane midplane

from the quiescent position:

$$\left\{ \begin{array}{l} \frac{D}{R^4} \nabla^4 w + \frac{\eta h^3}{12R^4} \nabla^4 \dot{w} + \rho h \ddot{w} = -p(t) - \gamma \dot{w} \\ w(1, t) = 0 \\ w'(1, t) = 0 \\ w(0, t) \neq \infty \\ w(\xi, 0) = 0 \\ \dot{w}(\xi, 0) = 0 \end{array} \right. \quad (8)$$

where  $\dot{w} = \partial w / \partial t$ ,  $w' = \partial w / \partial \xi$ ,  $\xi = r/R$  is the dimensionless radial coordinate,  $R$  is the radius of the membrane midplane,  $\rho$  is the PDMS density,  $h$  is the thickness of the membrane,  $\gamma = R_{hyd} \pi R^2$  is the damping coefficient of the channel,  $R_{hyd}$  is the hydrodynamic resistance of the channel.

$$D = \frac{Eh^3}{12(1 - \nu^2)}$$

where  $E$  is the PDMS Young modulus,  $\nu$  is Poisson's ratio. The boundary conditions mean the absence of transverse and rotational displacements on the boundary [29]. The membrane displacement is always finite. The initial conditions mean that all membranes were in quiescent position at  $t = 0$ .

A membrane pushes the liquid through the channel while being deformed. If flow is laminar, the reaction pressure in the channel is proportional to the volume flow rate which depends on the membrane velocity. The damping factor  $\gamma$  represents an averaged factor of proportionality between the channel reaction pressure and velocity of the liquid.

The applied pressure  $p(t)$  was calculated according to Section 3.1.

Problem (8) was solved using the eigenfunction expansion technique. Its solution has the following form:

$$w(\xi, t) = \sum_{n=1}^{+\infty} f_n(\xi) g_n(t) \quad (9)$$

where

$$f_n(\xi) = J_0(\lambda_n \xi) - \frac{J_0(\lambda_n)}{I_0(\lambda_n)} I_0(\lambda_n \xi) \quad (10)$$

are the eigenfunctions of the corresponding Sturm–Liouville problem ( $J_n$  are Bessel functions of the first kind,  $I_n$  are modified Bessel functions of the first kind.) Eigenvalues  $\lambda_n$  were obtained as a solution of the following equation

$$J_0(\lambda_n) I_1(\lambda_n) + I_0(\lambda_n) J_1(\lambda_n) = 0$$

A substitution of expansion (9) into (8) gave the following initial value problem to obtain the functions  $g_n(t)$ :

$$\left\{ \begin{array}{l} \ddot{g}_n + 2\beta_n \dot{g}_n + \omega_{0n}^2 g_n = -\frac{Q_n}{\rho h} p(t) \\ g_n(0) = 0 \\ \dot{g}_n(0) = 0 \end{array} \right. \quad (11)$$

where

$$\beta_n = \frac{\eta h^2 \lambda_n^4}{24 R^4 \rho} + \frac{\gamma}{2 \rho h} \quad \omega_{0n} = \sqrt{\frac{D}{\rho h}} \left( \frac{\lambda_n}{R} \right)^2$$

$$Q_n = \frac{2}{\lambda_n} \frac{J_1(\lambda_n) - \frac{J_0(\lambda_n)}{I_0(\lambda_n)} I_1(\lambda_n)}{J_1^2(\lambda_n) + \left( \frac{J_0(\lambda_n)}{I_0(\lambda_n)} \right)^2 I_1^2(\lambda_n)}$$

( $Q_n p(t)$  are the expansion coefficients of the pressure  $p(t)$  in the eigenfunctions  $f_n(\xi)$ ). Problem (11) represents a well-studied damped harmonic oscillator equation with zero initial conditions. Its solution can be found either numerically or using Green's function:

$$g_n(t) = -\frac{Q_n}{\rho h} \int_0^t e^{-\beta_n(t-\tau)} \frac{\sin[\omega_n(t-\tau)]}{\omega_n} p(\tau) d\tau \quad (12)$$

Thus, the deflection of the membrane midplane from its quiescent position is described by the following dependency

$$w(\xi, t) = -\sum_{n=1}^{+\infty} \frac{Q_n}{\rho h} \left[ J_0(\lambda_n \xi) - \frac{J_0(\lambda_n)}{I_0(\lambda_n)} I_0(\lambda_n \xi) \right] \times$$

$$\int_0^t e^{-\beta_n(t-\tau)} \frac{\sin[\omega_n(t-\tau)]}{\omega_n} p(\tau) d\tau \quad (13)$$

### 100 3.3. Volume flow rate

The volume flow is defined as an integration of the obtained membrane velocity over its surface:

$$Q(t) = \int_S \dot{w}(\xi, t) dS \quad (14)$$

To solve this integral curvilinear coordinates were used:

$$x = \xi \cos \varphi \quad y = \xi \sin \varphi \quad z = w(\xi, t)$$

with the following surface area element ([30])

$$dS = \xi \sqrt{1 + (w'(\xi, t))^2} d\xi d\varphi$$

Finally, the volume flow rate has the following form:

$$Q(t) = 2\pi \int_0^1 \dot{w}(\xi, t) \xi \sqrt{1 + (w'(\xi, t))^2} d\xi \quad (15)$$

The chamber membrane is able to reach the channel bottom on the downward motion. The integration lower limit is replaced by  $\xi_0(t)$  for this case, being the solution of

$$w(\xi_0, t) = -z_0$$

where  $z_0$  is the height of the channel.

All given calculations have been implemented in C++ using the Boost library to work with Bessel functions.

#### 4. Experimental setup

The experimental setup is shown schematically in Fig. 6. Each pump was connected to the Hemule control unit “8” using FESTO PUN-H-2×0.4 pneumatic tubes. The same tubes were used to connect inlet “3” and outlet “4” of the pump with reservoirs filled with deionized water “5”. Honeywell 40PC001B pressure sensors “2” were placed as shown in Fig. 1. Their readings were captured by a Tektronix MSO 3024 oscilloscope and converted to pressure units according to the sensor datasheet. The obtained pressure difference  $\Delta p(t)$  was converted to the volume flow rate as follows

$$Q(t) = \Delta p(t) \frac{Q_{av}}{\frac{1}{2T} \int_{t_0}^{t_0+T} \Delta p(t) dt}$$

105 where  $Q_{av}$  is the average volume flow rate. In order to measure it, the reservoir connected to the outlet of the pump was placed on an OHAUS EX 224 precision balance “7”. The reservoir was filled with mineral oil “6” to prevent the evaporation of the water from the surface. Division by 2 is caused by the fact that the unclosed pump connection scheme was used in the experiment.

110 The slope of pressure pulses over the membranes was adjusted by FESTO GRLO-M5-QS-3-LF-C throttles “9” mounted on a pneumatic tubes. The same throttle was used on the outlet tube to simulate the adjustment of friction loss of the microfluidic channel.

#### 5. Results and discussion

115 Measurements of the volume flow rate were carried out for all versions of the pump. The hydrodynamic resistances were estimated according to [31] and are about 280 Pa·s/mm<sup>3</sup> for a channel part between an outlet and a chamber and about 220 Pa·s/mm<sup>3</sup> for a part between an outlet and a valve. PDMS viscosity was taken to be 32 kPa·s [32]. Experimental results (Fig. 7) show that valves  
 120 with a smaller diameter produce peaks with a smaller magnitude (pump I and pump II), whereas the working chamber with a thinner membrane produces a higher peak (pump I and pump III). These results are in close agreement with theoretical predictions (Fig. 8). Some discrepancy between the theory and the experiment is observed when a valve opens. It happens probably due to the non-  
 125 laminar transitional flow when the strap of a valve is detached from the bottom

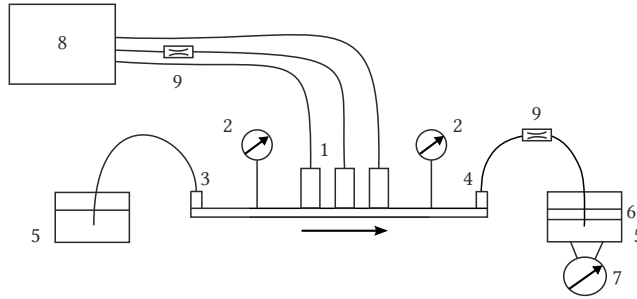


Figure 6: The scheme of the experimental setup: 1 – pump, 2 – pressure sensors, 3 – inlet, 4 – outlet, 5 – water reservoirs, 6 – oil layer, 7 – balance, 8 – control unit, 9 – throttles

of the channel and the fluid flows under it. Consideration of this transition process is beyond the scope of this paper.

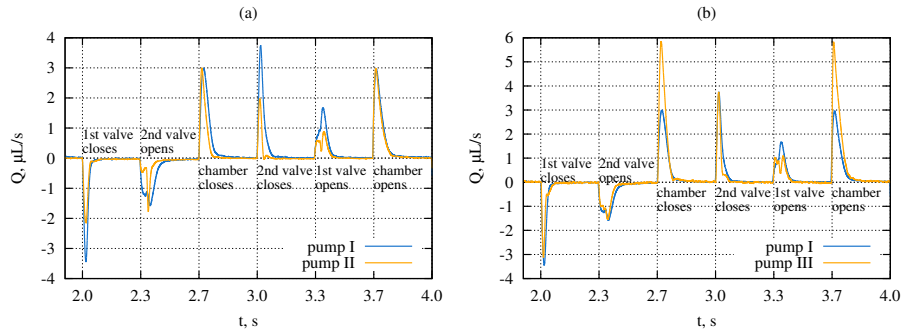


Figure 7: Comparison of volume flow rates generated by (a) pump I and pump II (smaller valves) and (b) pump I and pump III (thinner working chamber membrane)

Average volume flow rates over one pumping cycle for all types of the pump and for different control unit modes are represented in Fig. 9. As follows from these results, the average volume flow rate is proportional to the pumping frequency and the pressure magnitude until the chamber membrane reaches the channel bottom. The theoretically predicted average volume flow rates are equal for pump I and pump II because the contributions of valves compensate for each other if the valve properties are identical. The measured data coincides within a measurement error.

Fig. 10 represents theoretical dependencies of flow rate peak created by the chamber membrane with different pump parameters. The investigated parameters were the membrane radius (Fig. 10a) and thickness (Fig. 10b), as well as the hydraulic resistance of the channel after the pump (Fig. 10c) and the slope of the air pressure pulse over the membrane (Fig. 10d). The last was governed

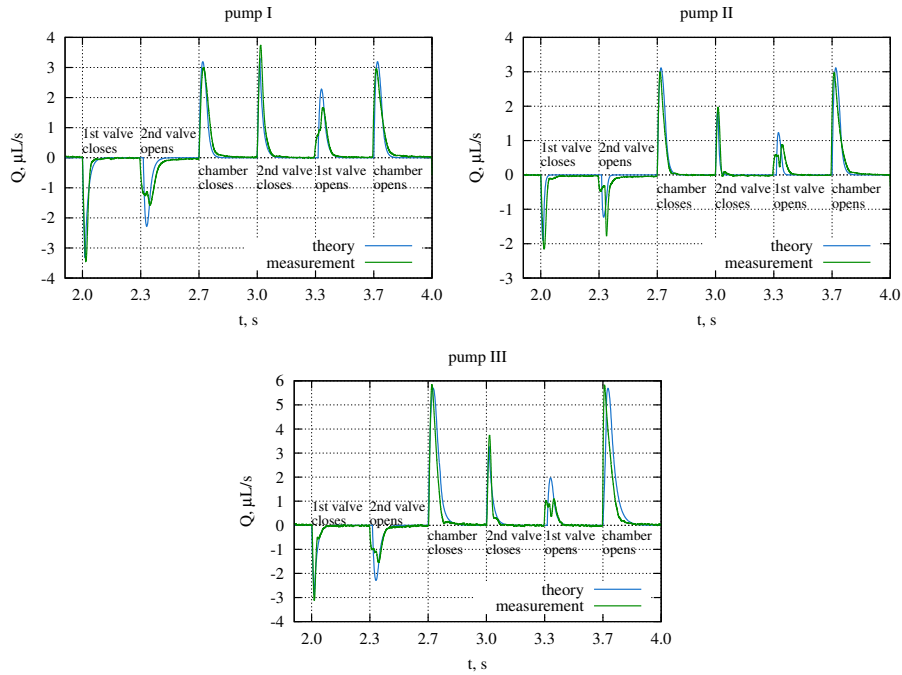


Figure 8: Comparison between the experimental results and the theoretical predictions

by throttles connected to the control unit outputs. (The smaller the throttle orifice, the gentler the slope.)

A curve break corresponds to the membrane reaching the bottom of the channel. The experimental evidence for the influence of the membrane radius and thickness on the peak form can be seen in Fig. 7 and 8. The qualitative experimental dependency of the peak on the hydrodynamic resistance of a channel is shown in Fig. 11. The hydrodynamic resistance was changed by varying the cross-section of the throttle connected to the outlet. Such throttle does not influence data obtained from a sensor placed closer to the inlet, therefore only the data from the sensor placed closer to the outlet is shown. The obtained curve represents the contribution to the flow rate of a valve nearest to the sensor and a chamber when this valve is open.

Similar measurements were carried out in order to study the dependency of the peak on the pressure slope. The latter is determined by a pneumatic tube orifice (Section 3.1) and was changed with a throttle mounted on a pneumatic tube, that operates the pressure over the membrane of the chamber. The corresponding data from a sensor placed closer to the pump outlet is shown in Fig. 12. All measurements were made using pump III.

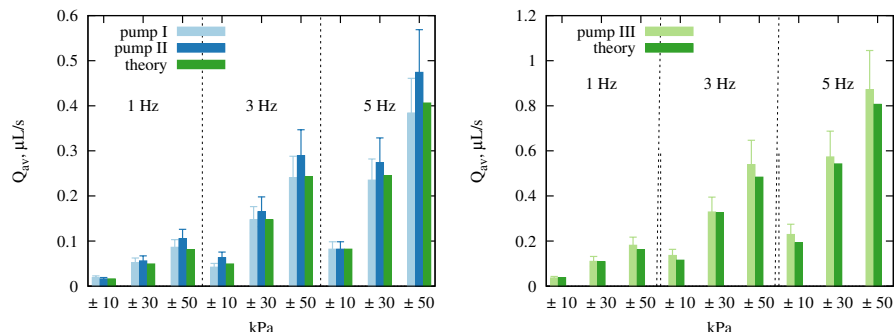


Figure 9: The average volume flow rate of investigated pumps compared with theory

## 6. Conclusion

160 The developed mathematical model provides the volume flow rate created  
 by a peristaltic-like displacement micropump with active valves by a point-  
 blank description of the membrane motion. The material of the membrane  
 (PDMS) was assumed to be isotropic, viscoelastic and was described using the  
 Kelvin-Voigt model. The hydrodynamic resistance of a microfluidic channel was  
 165 also considered. A number of assumptions were made in order to simplify the  
 solution. Namely, the channel walls were assumed to be stiff, the valves were  
 expected to fully stop when their strap reached the bottom of the channel, and  
 in this case the velocity of the chamber membrane was considered equal to zero.  
 The predictions of the model are in a good agreement with experimental results.  
 170 The main advantage of the developed model is the fact that it only uses the  
 physical parameters of the pump and allows the estimation of their influence on  
 the resulting flow. On the other hand it does not require sophisticated software  
 for implementation. The model can be used to describe other pumps working  
 on a similar principle and to obtain boundary conditions when calculating flow  
 175 in microfluidic channels. Since the calculation performed in Section 3.2 did not  
 use an explicit form of the applied pressure  $p(t)$ , one can substitute any other  
 force into the right-hand side of the equation and thus use this model to describe  
 pumps with other actuation types.

- 180 [1] D. Huh, B. D. Matthews, A. Mammoto, M. Montoya-Zavala, H. Y. Hsin,  
 D. E. Ingber, Reconstituting Organ-Level Lung Functions on a Chip, *Science* 328 (5986) (2010) 1662–1668. doi:10.1126/science.1188302.
- [2] D. Huh, G. A. Hamilton, D. E. Ingber, From 3D cell culture to organs-on-chips, *Trends Cell Biol.* 21 (12) (2011) 745–754. doi:10.1016/j.tcb.2011.09.005.
- 185 [3] M.-H. Wu, S.-B. Huang, G.-B. Lee, Microfluidic cell culture systems for  
 drug research, *Lab Chip* 10 (8) (2010) 939–956. doi:10.1039/b921695b.

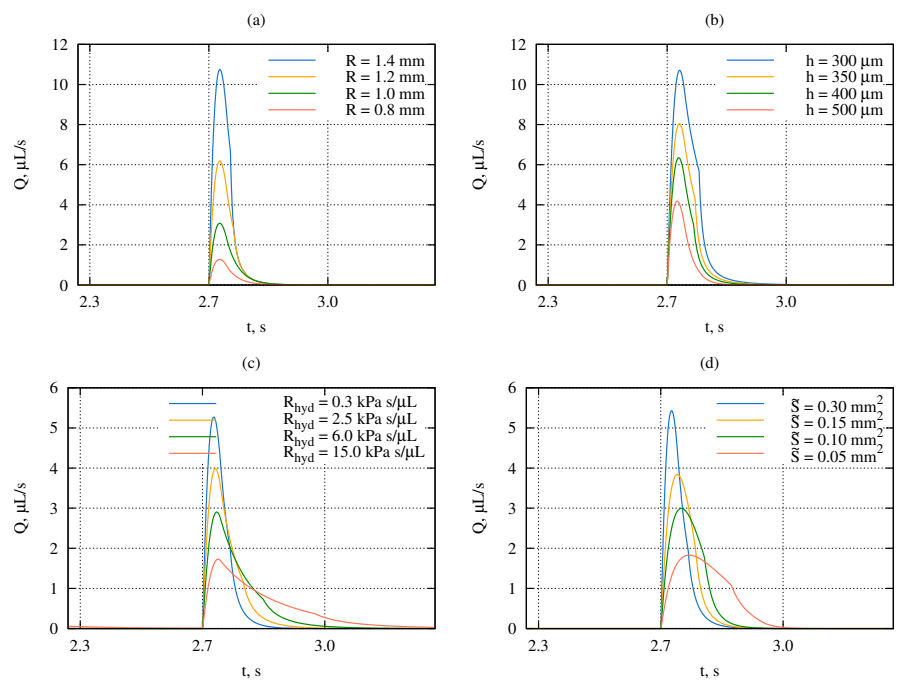


Figure 10: The impact of a membrane radius (a), its thickness (b), hydrodynamic resistance of a channel (c) and the slope of the pressure pulse (determined by  $\tilde{S}$ ) on the form of the peak created by the chamber of pump III

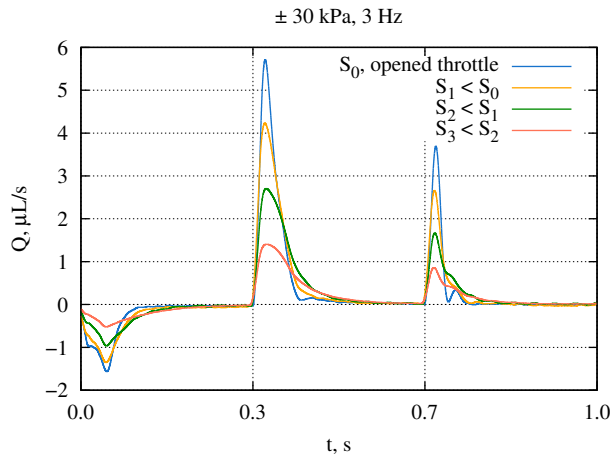


Figure 11: The throttle is mounted on the outlet to increase the hydrodynamic resistance after the pump. The Figure shows peaks obtained from the outlet pressure sensor for different throttle cross-sections.

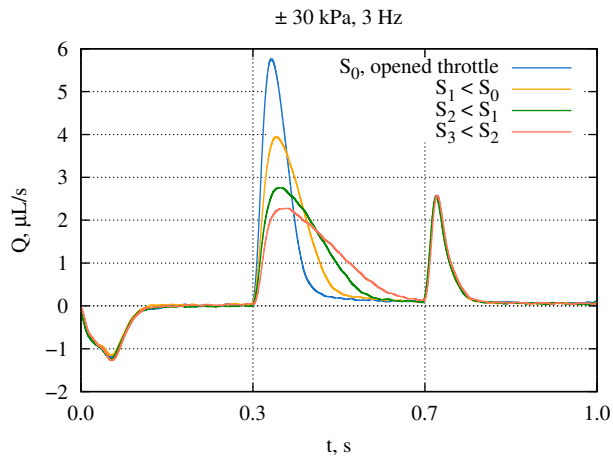


Figure 12: The slope of the pressure pulse is changed by varying the control unit throttle cross-section. The Figure shows peaks obtained from the outlet pressure sensor for different throttle cross-sections.

[4] D. J. Laser, J. G. Santiago, A review of micropumps, *J. Micromechanics Microengineering* 14 (6) (2004) R35–R64. doi:10.1088/0960-1317/14/6/R01.

190 [5] B. D. Iverson, S. V. Garimella, Recent advances in microscale pumping

- technologies: a review and evaluation, *Microfluid. Nanofluidics* 5 (2) (2008) 145–174. doi:10.1007/s10404-008-0266-8.
- [6] S.-B. Huang, S.-S. Wang, C.-H. Hsieh, Y. C. Lin, C.-S. Lai, M.-H. Wu, An integrated microfluidic cell culture system for high-throughput perfusion three-dimensional cell culture-based assays: effect of cell culture model on the results of chemosensitivity assays., *Lab Chip* 13 (6) (2013) 1133–1143. doi:10.1039/c2lc41264k.
- [7] C. Jacobs, C. Yellowley, B. Davis, Z. Zhou, J. Cimbala, H. Donahue, Differential effect of steady versus oscillating flow on bone cells, *J. Biochem* 31 (11) (1998) 969–976. arXiv:NIHMS150003, doi:10.1016/j.biotechadv.2011.08.021.Secreted.
- [8] T. K. Hsiai, S. K. Cho, H. M. Honda, S. Hama, M. Navab, L. L. Demer, C. M. Ho, Endothelial cell dynamics under pulsating flows: Significance of high versus low shear stress slew rates, *Ann. Biomed. Eng.* 30 (5) (2002) 646–656. doi:10.1114/1.1484222.
- [9] M. T. van der Pauw, J. Klein-Nulend, T. van den Bos, E. H. Burger, V. Everts, W. Beertsen, Response of periodontal ligament fibroblasts and gingival fibroblasts to pulsating fluid flow: nitric oxide and prostaglandin E2 release and expression of tissue non-specific alkaline phosphatase activity, *J Periodontal Res* 35 (6) (2000) 335–343. doi:10.1034/j.1600-0765.2000.035006335.x.
- [10] W.-Y. Lin, Y.-H. Chang, H.-Y. Wang, T.-C. Yang, T.-K. Chiu, S.-B. Huang, M.-H. Wu, The study of the frequency effect of dynamic compressive loading on primary articular chondrocyte functions using a micro-cell culture system, *BioMed Research Int.* 2014 (1) (2014) 762570–762582. doi:10.1155/2014/762570.
- [11] C. Deبادi, P. J. Ravi, L. Yeo, J. Friend, Fluid-Structure Interaction in Deformable Microchannels, *Phys. Fluids* 24 (2012) 102002 – 102037. arXiv:arXiv:1203.6427v1, doi:10.1063/1.4759493.
- [12] O. O. Osman, A. Shirai, S. Kawano, A numerical study on the performance of micro-vibrating flow pumps using the immersed boundary method, *Microfluid. Nanofluidics* 19 (3) (2015) 595–608. doi:10.1007/s10404-015-1586-0.
- [13] F. Goldschmidtböing, A. Doll, M. Heinrichs, P. Woias, H.-J. Schrag, U. T. Hopt, A generic analytical model for micro-diaphragm pumps with active valves, *J. Micromechanics Microengineering* 15 (4) (2005) 673–683. doi:10.1088/0960-1317/15/4/001.
- [14] C. Yang, D. Hu, B. Sun, X. Cui, Q. Zhu, R. H. W. Lam, Mixing in an enclosed microfluidic chamber through moving boundary motions, *Microfluid. Nanofluidics* 19 (3) (2015) 711–720. doi:10.1007/s10404-015-1596-y.

- [15] T. Bourouina, J.-P. Grandchamp, Modeling micropumps with electrical equivalent networks, *J. Micromechanics Microengineering* 6 (4) (1996) 398–404. doi:10.1088/0960-1317/6/4/006.
- 235 [16] E. Morganti, I. Fuduli, A. Montefusco, M. Petasecca, U. G. Pignatelli, SPICE modelling and design optimization of micropumps, *Int. J. Environ. Anal. Chem.* 85 (9-11) (2005) 687–698. doi:10.1080/03067310500153876.
- [17] J. Goulpeau, D. Trouchet, A. Ajdari, P. Tabeling, Experimental study and modeling of polydimethylsiloxane peristaltic micropumps, *J. Appl. Phys.* 98 (4) (2005) 1–9. doi:10.1063/1.1947893.
- 240 [18] C.-W. Huang, S.-B. Huang, G.-B. Lee, Pneumatic micropumps with serially connected actuation chambers, *J. Micromechanics Microengineering* 16 (11) (2006) 2265–2272. doi:10.1088/0960-1317/16/11/003.
- 245 [19] S. Bendib, O. Francais, Analytical study of microchannel and passive microvalve : “Application to Micropump simulator”, in: *Des. Charact. Packag. Mems Microelectron. Ii*, Vol. 4593, 2001, pp. 283–291. doi:10.1117/12.448859.
- [20] O. T. Nedelcu, J.-L. Morelle, C. Tibeica, S. Voccia, I. Codreanu, S. Dahms, Modelling and simulation of a pneumatically actuated micropump, in: *Semicond. Conf. 2007. CAS 2007. Int.*, Vol. 1, 2007, pp. 77 – 80.
- 250 [21] M. Busek, M. Nötzel, C. Polk, F. Sonntag, Characterization and simulation of peristaltic micropumps, *J. Sensors Sens. Syst.* 2 (2) (2013) 165–169. doi:10.5194/jsss-2-165-2013.
- 255 [22] M. A. Unger, H.-P. Chou, T. Thorsen, A. Scherer, S. R. Quake, Monolithic Microfabricated Valves and Pumps by Multilayer Soft Lithography, *Science* 288 (2000) 113–116.
- [23] M. J. Owen, J. L. Stasser, Plasma treatment of polydimethylsiloxane, *J. Adhes. Sci. Technol.* 8 (10) (1994) 1063–1075. doi:10.1163/156856194X00942.
- 260 [24] I. D. Johnston, D. K. McCluskey, C. K. L. Tan, M. C. Tracey, Mechanical characterization of bulk Sylgard 184 for microfluidics and microengineering, *J. Micromechanics Microengineering* 24 (3) (2014) 035017 – 035024. doi:10.1088/0960-1317/24/3/035017.
- [25] J. N. Reddy, *Theory and Analysis of Elastic Plates and Shells*, 2nd Edition, CRC Press, 2006.
- 265 [26] D. Armani, C. Liu, N. Aluru, Re-configurable fluid circuits by PDMS elastomer micromachining, in: *Twelfth IEEE Int. Conf. Micro Electro Mech. Syst.*, 1999, pp. 222–227. doi:10.1109/MEMSYS.1999.746817.

- [27] M. Z. Kolovsky, *Nonlinear Dynamics of Active and Passive Systems of Vibration Protection*, Springer-Verlag Berlin Heidelberg, 1999.
- 270 [28] S. B. Singh, M. Arif, Vibration analysis of visco-elastic clamped circular plates subjected to thermal gradient, *Indian J. Eng. Matherial Sci.* 9 (5) (2002) 103–108.
- [29] R. Sircar, Dynamic response of circular plates on elastic foundation subjected to sonic booms, *Indian J. Pure Appl. Math.* 6 (5) (1973) 530–538.
- 275 [30] G. M. Fichtenholz, *The fundamentals of mathematical analysis*, Oxford : Pergamon, 1965.
- [31] H. Bruus, *Theoretical Microfluidics*, Oxford University Press, 2008.
- [32] F. E. Swallow, Viscosity of polydimethylsiloxane gum: Shear and temperature dependence from dynamic and capillary rheometry, *J. Appl. Polym. Sci.* 84 (13) (2002) 2533–2540. doi:10.1002/app.10563.
- 280